New Reconstructions of the (110) Surface of Rutile TiO_2 Predicted by an Evolutionary Method

Qinggao Wang,[1,3,*] Artem R. Oganov,[2,1,4] Qiang Zhu,[2] and Xiang-Feng Zhou[2]
[1]*Moscow Institute of Physics and Technology, 9 Institutskiy Lane, Dolgoprudny City, Moscow Region 141700, Russia*
[2]*Department of Geosciences and Center for Materials by Design, Stony Brook University, Stony Brook, New York 11794, USA*
[3]*Department of Physics and Electrical Engineering, Anyang Normal University, Anyang, Henan Province 455000, People's Republic of China*
[4]*School of Materials Science and Engineering, Northwestern Polytechnical University, Xi'an, Shanxi 710072, People's Republic of China*
(Received 29 June 2014; published 24 December 2014)

Reconstructions of the (110) surface of rutile TiO_2 (the dominant surface of this important mineral and catalyst) are investigated using the evolutionary approach, resolving previous controversies. Depending on thermodynamic conditions, four different stable reconstructions are observed for this surface. We confirm the recently proposed "Ti_2O_3-(1×2)" and "Ti_2O-(1×2)" reconstructions and predict two new reconstructions "Ti_3O_2-(1×2)" and "Ti_3O_3-(2×1)," which match experimental results. Furthermore, we find that surface electronic states are sensitive to reconstructions and, therefore, depend on thermodynamic conditions.

DOI: 10.1103/PhysRevLett.113.266101 PACS numbers: 68.35.Rh, 68.35.B-, 68.47.Fg, 71.15.Mb

TiO_2 nanocrystals and low-dimensional materials are widely applied in the remediation of pollutants and photoelectron chemical conversion of solar energy [1,2]. In these applications, surface structures are the key to understanding reactivity and reaction mechanisms [3,4]. After sputtering or annealing samples in high vacuum at different temperatures, the rutile $TiO_2(110)$ surface reconstructs to (1×1) [5,6], single-linked (1×2) [7–9], cross-linked (1×2) [10,11], and pseudohexagonal rosette structures [12]. However, the exact atomic configurations are under debate, and this uncertainty hampers the understanding of related photocatalytic reactions.

Two models are being considered for the single-linked (1×2) reconstruction. The "Ti_2O_3-(1×2)" model adding Ti_2O_3 stripes along the [001] direction was originally proposed by Onishi *et al.* [7,9]. However, later, the "Ti_2O-(1×2)" model adding Ti_2O stripes along the [001] direction was proposed by Park *et al.* [5,6]. The Ti_2O_3-(1×2) model was confirmed by low-energy electron diffraction investigations [8,13], while the Ti_2O-(1×2) model was supported by a transmission electron microscopy investigation [14]. Consequently, atomic structures of the single-linked (1×2) reconstruction are under debate.

The formation of the cross-linked (1×2) reconstruction requires higher temperature than that of the single-linked (1×2) reconstruction [10], corresponding to an environment with a lower O chemical potential. From the thermodynamic viewpoint, the cross-linked (1×2) reconstruction should be more O deficient. However, the proposed "Ti_3O_6-(1×2)" model [10] losing an O-Ti-O unit is stoichiometric, which appears counterintuitive. In a previous study, the rosette reconstruction was regarded as an incomplete TiO_2 layer [12], but the atomic structure was not fully resolved. Therefore, atomic structures of the single-linked (1×2), cross-linked (1×2), and rosette reconstructions are questionable.

To resolve these controversies, we performed a systematic study, searching for stable surface structures using the USPEX code [15–18], which has been successfully applied for predicting stable structures of bulk crystals [16], nanoclusters [17], surfaces [18], and polymers [19]. As a global optimization method, the USPEX code uses three ways (heredity, mutation, and transmutation) to produce next-generation surface structures, and the whole prediction requires hundreds or thousands of individual structure relaxations [18]. Each candidate surface structure is divided into vacuum, surface region, and substrate, and only the surface region is optimized [18]. In this way, surface structures can be explored efficiently, allowing for both structural and compositional variation.

In our calculations, at most, four multiplications of the unit cell (namely, $1*1$, $1*2$, $2*1$, $1*3$, $3*1$, $2*2$, $1*4$, and $4*1$) were considered, and maximally, two Ti and four O atoms were allowed for per surface unit cell. Each of the supercells contained a vacuum layer of 13 Å and a substrate slab of 4–5 TiO_2 layers with the top region of 3.5 Å being relaxed. We explored 1791 structures, or 40 generations, in the whole structure search. These structures were ranked according to the well-designed fitness function of Ref. [18]; the found structures contained added stripes (e.g., TiO, TiO_2, Ti_2O, Ti_3O_2, Ti_2O_3, or Ti_3O_3) and defects (such as O vacancy or Ti interstitial). Low-energy structures were selected for detailed analysis. The additional low-energy structures are given in the Supplemental Material [20], which may be observed experimentally . Slabs and the vacuum layer were increased to 6–7 TiO_2 layers and 15 Å,

respectively, and only the bottom layer was kept fixed to obtain more accurate surface energies. In addition, symmetric slabs were adopted to characterize electronic structures.

During the structure search and postprocessing, structure relaxation was done by spin-polarized calculations using the VASP package [21,22], since ground states of rutile $TiO_{2-x}(110)$ systems can be ferromagnetic [23]. We used the generalized gradient approximation (GGA) in the Perdew-Burke-Ernzerhof form [24], with the addition of a Hubbard U term ($U = 4.1$ eV) to deal with the self-interaction error of the GGA [23]. The projector-augmented wave method was applied to treat core electrons [25], while valence orbitals were expanded in the basis of plane waves. For Brillouin zone sampling, we used uniform Γ-centered meshes with reciprocal-space resolution of $2\pi \times 0.09$ Å^{-1}. Relaxation proceeded until net forces on all atoms were below 0.001 eV/Å. Moreover, dipole corrections were adopted to cancel the interactions between the slab and its periodic images [26,27].

Surface energy, which determines stability of a surface, is defined as

$$\Delta G = \frac{1}{N}\left[G_{\mathrm{sur}} - \sum_i n_i \mu_i\right], \tag{1}$$

where G_{sur} is the Gibbs free energy of a candidate structure. n_i and μ_i are the number of atoms and chemical potential for each atomic species, respectively. N is equal to $(m \times n)$ for an $(m * n)$ surface cell and serves as a normalization factor.

The Gibbs free energy of a solid phase can be replaced by its internal energy, because the contributions of temperature and ambient pressure are negligible [28]. Chemical potentials (μ_{o} and μ_{Ti}) satisfy the following boundary conditions: (i) $\mu_{\mathrm{o}} \le \frac{1}{2}\mu_{\mathrm{o}_2}$, (ii) $\mu_{\mathrm{Ti}} \le \mu_{\mathrm{Ti}}^{\mathrm{bulk}}$, and (iii) $\mu_{\mathrm{Ti}} + 2\mu_{\mathrm{o}} = E_{\mathrm{TiO}_2}$, in which E_{TiO_2} is the internal energy of the bulk rutile TiO_2 unit cell. Accordingly, Eq. (1) is rewritten as

$$\Delta G = \frac{1}{N}[E_{\mathrm{sur}} - n_{\mathrm{Ti}} E_{\mathrm{TiO}_2} - \mu_{\mathrm{o}}(n_{\mathrm{o}} - 2n_{\mathrm{Ti}})], \tag{2}$$

where E_{sur} is the internal energy of the candidate structure.

In equilibrium with O_2 gas, μ_{o} is expressed as [29]

$$\mu_{\mathrm{o}} = \frac{1}{2}\left[E_{\mathrm{o}_2} + \Delta H_{\mathrm{o}_2}(T, P^0) - T\Delta S_{\mathrm{o}_2}(T, P^0) + k_B T \ln\left(\frac{P}{P^0}\right)\right] = \frac{1}{2}E_{\mathrm{o}_2} + \Delta\mu_{\mathrm{o}}(T, P), \tag{3}$$

where k_B, P^0, and P are the Boltzmann constant, standard atmospheric pressure, and oxygen partial pressure, respectively. E_{o_2} was obtained from a spin-polarized calculation. $\Delta H_{\mathrm{o}_2}(T, P^0)$ and $T\Delta S_{\mathrm{o}_2}(T, P^0)$ were taken from a thermodynamic database [30]. The fourth term is the contribution coming from the partial pressure of oxygen. Dependence of surface energies on the chemical potential of oxygen (where a straight line corresponds to each structure) is shown in Fig. 1(a). Stable structures are those that have the lowest surface energy at a certain range of chemical potentials.

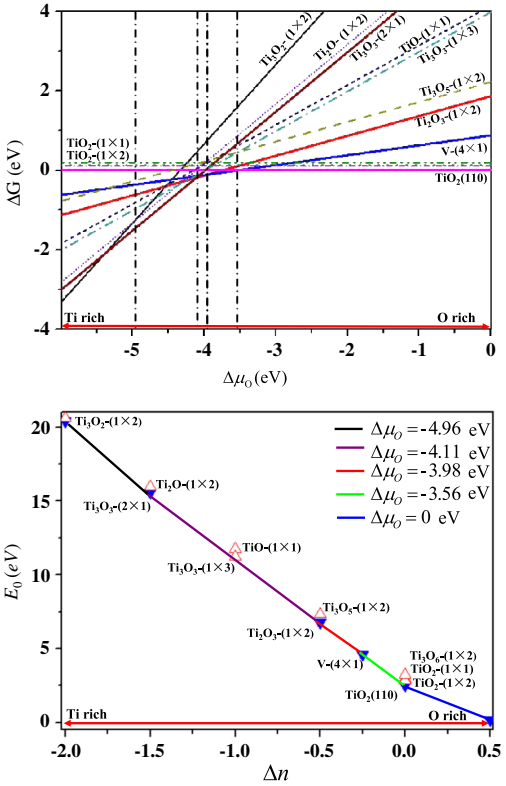

FIG. 1 (color online). Surface phase diagram of rutile $TiO_2(110)$: stability of different structures as a function of (a) oxygen chemical potential $\Delta\mu_{\mathrm{o}}$ and (b) stoichiometry deviation Δn. Surface energies in (a) are relative to the unreconstructed (110) surface. Stable and metastable structures in (b) are represented by solid and hollow triangles, respectively.

We can recast Fig. 1(a) in another insightful form by defining μ_{Ti}-independent (E_0) and stoichiometry deviation (Δn) terms as

$$E_0 = \frac{1}{N}[E_{\mathrm{sur}} - n_{\mathrm{Ti}} E_{\mathrm{TiO}_2}] \quad \text{and} \quad \Delta n = \frac{1}{N}(n_{\mathrm{o}} - 2n_{\mathrm{Ti}}), \tag{4}$$

respectively. In the resulting $E_0(\Delta n)$ plot [Fig. 1(b)], each of the surface structures is represented as a point, and stable structures (points) form a convex hull. Points above the convex hull represent metastable structures.

Figure 1 shows that there are four stable structures: the unreconstructed rutile $TiO_2(110)$ (-3.56 eV $\le \Delta\mu_{\mathrm{o}} \le 0$ eV), "V-(4×1)" (-3.98 eV $\le \Delta\mu_{\mathrm{o}} \le -3.56$ eV), Ti_2O_3-(1×2) (-4.11 eV $\le \Delta\mu_{\mathrm{o}} \le -3.98$ eV), and "Ti_3O_3-(2×1)" (-4.96 eV $\le \Delta\mu_{\mathrm{o}} \le -4.11$ eV). A number of interesting metastable structures were also predicted, e.g., "Ti_3O_2-(1×2)" and Ti_2O-(1×2) reconstructions.

There exists a stability field for the unreconstructed rutile $TiO_2(110)$ surface, which shows (1×1) bulklike termination ($\Delta n = 0$), in agreement with previous investigations

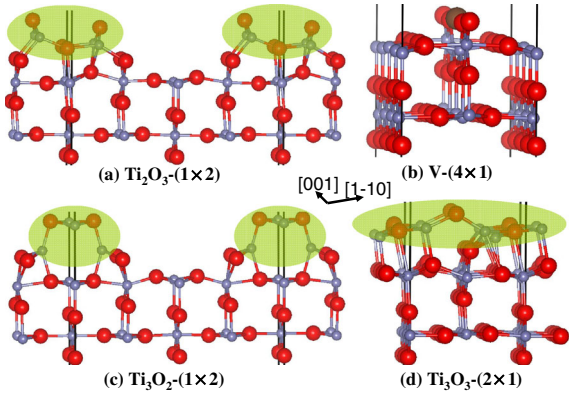

FIG. 2 (color online). Side views of stable structures of rutile $TiO_2(110)$: (a) Ti_2O_3-(1×2), previously proposed in Refs. [7,9], (b) V-(4×1), (d) Ti_3O_3-(2×1), as well as (c) metastable Ti_3O_2-(1×2). Ti and O atoms are represented by small gray and big red balls, respectively. An O vacancy in V-(4×1) is represented by the dark gray ball. Structural features are highlighted by yellow shades.

[31,32]. V-(4×1) is a reduced rutile $TiO_2(110)$ surface ($\Delta n = -0.25$), containing a bridge oxygen vacancy [Fig. 1(b)]. Such defects were observed experimentally [23]. The predicted Ti_2O_3-(1×2) reconstruction ($\Delta n = -0.5$) adding Ti_2O_3 stripes along the [001] direction is identical to the earlier proposed model [7–9,13]. As to the predicted Ti_3O_3-(2×1) reconstruction [Fig. 2(d)] ($\Delta n = -1$), its predicted dimensions are 6.5 and 6 Å along the [1–10] and [001] directions, respectively, which are the same as those of the rosette reconstruction [12], and we propose Ti_3O_3-(2×1) to be the atomic configuration of the rosette reconstruction. Surface stoichiometries of our predicted reconstructions (Δn: $0 \rightarrow -1$) systematically change as a function of O chemical potential ($\Delta\mu_o$: $0 \rightarrow -4.96$ eV) from the unreconstructed rutile $TiO_2(110)$ to V-(4×1) to Ti_2O_3-(1×2) to Ti_3O_3-(2×1). Clearly, surface reconstructions depend on thermodynamic conditions.

At each given stoichiometry, the stable structure tends to minimize the number of dangling bonds, as revealed through the analysis of structural geometry. Taking Ti_3O_3-(2×1) as an example, more surface O atoms are three-coordinate than in the unreconstructed rutile $TiO_2(110)$ surface: O atoms in the bulk are also three-coordinate. Several metastable structures [e.g., Ti_3O_2-(1×2) [Fig. 2(c)], Ti_2O-(1×2) [Supplemental Material [20], Fig. 1(a)], "TiO-(1×1)" [Supplemental Material [20], Fig. 1(c)], and "Ti_3O_3-(1×3)" [Supplemental Material [20], Fig. 1(e)]] also have more surface O atoms in a threefold coordination, supporting our conclusion. As a wide-gap semiconductor, TiO_2 has mixed ionic-covalent bonding, and, thus, the driving force behind reconstructions is complex for different low-index surfaces. For example, Kubo *et al.* reported that the reduction of dangling bonds leads to a reconstruction for rutile $TiO_2(011)$ [33], while Lazzeri and Selloni concluded that the reconstruction of anatase $TiO_2(001)$ is stress driven [34]. The rutile $TiO_2(110)$ has the lowest density of dangling bonds [33]. Therefore, stoichiometry deviations are necessary to cause reconstructions of rutile $TiO_2(110)$.

Ti_2O-(1×2) reconstruction adding Ti_2O stripes along the [001] direction is the same as the proposed model [5,6,14]. The predicted Ti_3O_2-(1×2) [Fig. 2(c)] and TiO_2-(1×2) [Supplemental Material [20], Fig. 1(b)] contain added Ti_3O_2 and TiO_2 stripes along the [001] direction, respectively. The predicted structures of TiO-(1×1), TiO_2-(1×1) [Supplemental Material [20], Fig. 1(d)] and Ti_3O_3-(1×3), correspond to the observed (1×1) and (1×3) reconstructions in experiments, respectively [5,35].

Scanning tunneling microscopy (STM) images were simulated by calculating electronic density of states over an energy window above the Fermi level, as done in previous studies [35,36]. For O-deficient structures, Ti atoms at surface are imaged because the Fermi levels locate at conduction band minima [35,36]. Accordingly, the obtained structural information is attributed to the arrangement of Ti atoms. Therefore, we consider the heights ($H_{[110]}$) of the topmost Ti atoms relative to the underlying Ti-O layer and distances ($D_{[1-10]}$) between surface Ti rows along the [1–10] direction for Ti_2O_3-(1×2), Ti_3O_2-(1×2), and Ti_3O_3-(2×1) reconstructions.

The simulated STM image of Ti_2O_3-(1×2) [Fig. 3(a)] shows a single-linked pattern along the [1–10] direction, in agreement with the reported STM image of the single-linked (1×2) reconstruction [Fig. 3(b)] [35]. Simultaneously, its $H_{[110]}$ (2.87 Å) and $D_{[110]}$ (3.70 Å) agree well with the corresponding experimental values (Table I) [7,10]. Both Ti_2O_3-(1×2) and Ti_2O-(1×2) were argued to correspond to the atomic structure of the single-linked (1×2) reconstruction [5,6,8,13,14]. Certainly, the simulated STM image of Ti_2O-(1×2) reconstruction also shows a single-linked pattern, but unlike Ti_2O_3-(1×2), it is metastable.

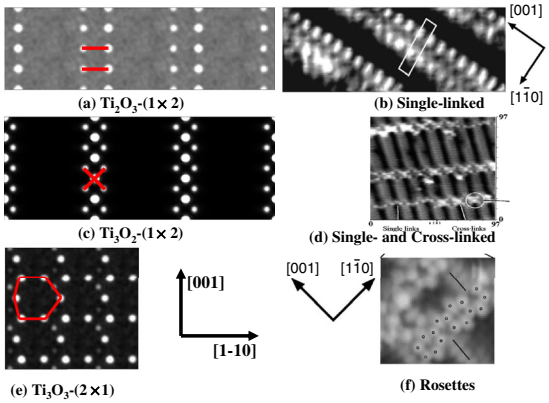

FIG. 3 (color online). Simulated STM images of (a) Ti_2O_3-(1×2), (c) Ti_3O_2-(1×2), and (e) Ti_3O_3-(2×1), where STM features are highlighted, as well as reported STM images of (b) single-linked (1×2) [35], (d) single- and cross-linked (1×2) [10], and (f) rosette reconstructions [12].

TABLE I. Heights ($H_{[110]}$) of the topmost Ti atoms relative to the underlying Ti-O layer and distances ($D_{[110]}$) between surface Ti atom rows along the [1–10] direction. "(exp)" denotes the corresponding experimental value.

Structure	$H_{[110]}$ (Å)	$H_{[110]}$ (exp)	$D_{[1-10]}$ (Å)	$D_{[1-10]}$ (exp)
Ti_2O_3-(1×2)	2.87	2.6–2.8 [10]	3.70	3.5–3.6 [7]
Ti_3O_2-(1×2)	4.19	4.0 [10]	...	...
Ti_3O_3-(2×1)	2.97	...	...	...

For the simulated STM image of Ti_3O_2-(1×2) [Fig. 3(c)], big bright round spots are surrounded by four small bright round spots together forming a cross-linked pattern, in agreement with the reported STM image of the cross-linked (1×2) reconstruction [Fig. 3(d)] [10]. Furthermore, its $H_{[110]}$ (4.19 Å) is close to the experimental value (4.0 Å) [10]. Experimentally, the temperature of formation of the cross-linked (1×2) reconstruction is higher than that of formation of the single-linked (1×2) reconstruction [10]. The cross-linked (1×2) reconstruction is more O deficient than the single-linked (1×2) reconstruction, favoring Ti_3O_2-(1×2) reconstruction over the earlier proposed Ti_3O_6-(1×2).

For completeness, the earlier proposed "Ti_3O_5-(1×2)" [35] and Ti_3O_6-(1×2) [10] models (Supplemental Material [20], 2) were analyzed, and these turned out to be unstable or metastable according to our calculations. The Ti_3O_5-(1×2) reconstruction has indeed been questioned [37]. The Ti_3O_6-(1×2) model [10,11] is similar to Ti_3O_5-(1×2): both of them lose one of the O-Ti-O units, and new dangling bonds make them unfavorable.

In the simulated STM image of Ti_3O_3-(2×1) [Fig. 3(e)], bright round spots form a distorted hexagonal pattern, which is the same as the reported STM image of the rosette reconstruction [Fig. 3(f)] [12]. As mentioned, the dimensions of Ti_3O_3-(2×1) are the same as those of the rosette reconstruction, and its $H_{[110]}$ (2.97 Å) is close to the reported value (about a monatomic step height, 3.24 Å) [12]. Consequently, Ti_3O_3-(2×1) is the rosette reconstruction.

Clearly, the predicted reconstructions agree with experimental results in STM patterns and structure parameters. Ideally, these reconstructions can be further confirmed by surface x-ray diffraction and transmission electron diffraction methods, which could provide atomic coordinates, such as on rutile $TiO_2(011)$ [38] and $TiO_2(100)$ [39]. To facilitate experimental studies, atomic fractional coordinates of the upper layers of the predicted reconstructions are given in the Supplemental Material [20].

Since $\Delta\mu_o$ is a function of temperature and pressure, stable surface structures of rutile $TiO_2(110)$ change with temperature and pressure, as shown in Fig. 4. Experimentally, the unreconstructed rutile $TiO_2(110)$ surface formed under conditions $\log(p/p^0) = -13$ and $1000 \le T \le 1100$ K [31], which just falls into the white region of Fig. 4. Bridge-O vacancies were observed

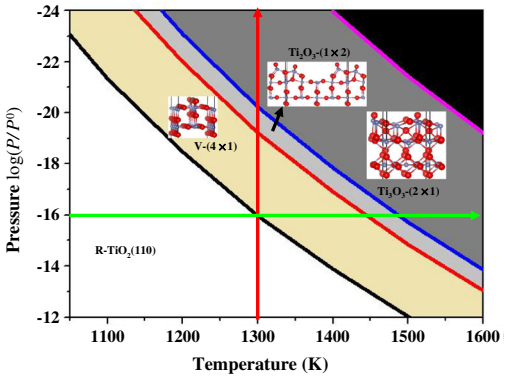

FIG. 4 (color online). Oxygen pressure-temperature phase diagram of the rutile $TiO_2(110)$ surface. Metal Ti deposition is favorable in the black region.

experimentally [23]. Here, they are demonstrated to have a stability field, since the V-(4×1) structure has a bridge-O vacancy.

Ti_2O_3-(1×2) is stable in a narrow temperature region (light blue region in Fig. 4). It should transform into Ti_3O_3-(2×1) upon increasing temperature or decreasing oxygen partial pressure. Experimentally, the single-linked (1×2) reconstruction [namely, Ti_2O_3-(1×2) or Ti_2O-(1×2)] transformed into the cross-linked (1×2) reconstruction [i.e., metastable Ti_3O_2-(1×2)] upon increasing temperature [10]. We interpret this transition as driven by kinetics.

The densities of states (DOS) and band structures of stable reconstructions are illustrated in Fig. 5. Compared with the unreconstructed rutile $TiO_2(110)$ surface, gap states appear for Ti_2O_3-(1×2), Ti_3O_2-(1×2), and Ti_3O_3-(2×1) reconstructions, corresponding to electrons localized at surface Ti atoms. In other words, rutile $TiO_2(110)$ reconstructions have surface Ti^{3+} ions, i.e., reduced Ti ions.

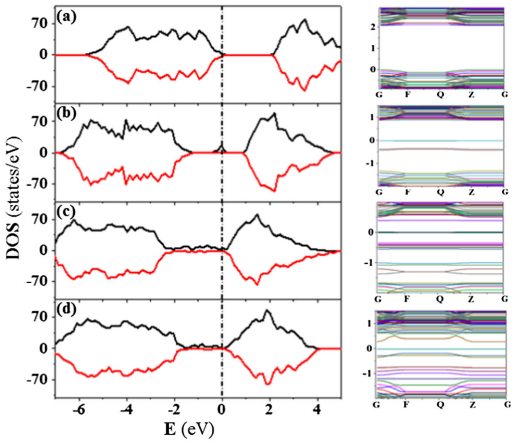

FIG. 5 (color online). DOS and band structures for (a) unreconstructed rutile $TiO_2(110)$, (b) Ti_2O_3-(1×2), (c) Ti_3O_2-(1×2), and (d) Ti_3O_3-(2×1), respectively. The vertical line at 0 eV is the Fermi level. The spin-up and -down states are represented by black and red lines, respectively.

The calculated band gap of bulk rutile TiO_2 is 2.3 eV, to be compared with the experimental value of 3.0 eV [40]. The band gap of unreconstructed rutile $TiO_2(110)$ is similar to that of bulk rutile TiO_2, being lower by just 0.2 eV. As shown in Fig. 5(b), deep donor energy levels are created for the Ti_2O_3-(1×2) reconstruction; these which are occupied states. For the heavier reduced reconstructions, more gap states are created, leading to further reduction of the band gap. The computed (corrected for GGA + U underestimation) band gaps of the Ti_3O_2-(1×2) and Ti_3O_3-(2×1) are 1.50 (2.20) and 1.00 (1.70) eV, respectively. In contact with the environment, these gap states would be changed because of the interactions with exterior molecules (e.g., H_2O molecules), due to orbital mixing and charge transfer. Therefore, environmental factors must be considered when investigating the effects of surface reconstructions on photocatalytic reactivity.

In conclusion, we present a complete and renewed understanding of stable reconstructions of rutile $TiO_2(110)$ surface. Ti_2O_3-(1×2) [8,13] and Ti_2O-(1×2) [5,14] are found to be stable and metastable structures of the single-linked (1×2) reconstruction, respectively. Our predicted Ti_3O_2-(1×2) and Ti_3O_3-(2×1) models correspond to the reported cross-linked (1×2) [10] and rosette [12] reconstructions, respectively. Our work resolves previous controversies on this subject and will play an important role in the related surface engineering and explanation of experimental results.

This research is supported by the government of the Russian Federation under Grant No. 14.A12.31.0003 and the "5top100" postdoctoral fellowship conducted at Moscow Institute of Physics and Technology (MIPT). Calculations were performed on the Rurik supercomputer of our laboratory at MIPT.

*Corresponding author.
wangqinggao1984@126.com

[1] C. L. Pang, R. Lindsayb, and G. Thornton, Chem. Soc. Rev. **37**, 2328 (2008).
[2] T. L. Thompson and J. T. Yates, Jr., Chem. Rev. **106**, 4428 (2006).
[3] C. L. Pang, O. Bikondoa, D. S. Humphrey, A. C. Papageorgiou, G. Cabailh, R. Ithnin, Q. Chen, C. A. Muryn, H. Onishi, and G. Thornton, Nanotechnology **17**, 5397 (2006).
[4] Y. Wang, Y. Ye, and K. Wu, J. Phys. Chem. B **110**, 17960 (2006).
[5] K. T. Park, M. H. Pan, V. Meunier, and E. W. Plummer, Phys. Rev. Lett. **96**, 226105 (2006).
[6] K. T. Park, M. Pan, V. Meunier, and E. W. Plummer, Phys. Rev. B **75**, 245415 (2007).
[7] H. Onishi and Y. Iwasawa, Surf. Sci. **313**, L783 (1994).
[8] M. Blanco-Rey, J. Abad, C. Rogero, J. Mendez, M. Lopez, J. Martin-Gago, and P. de Andres, Phys. Rev. Lett. **96**, 055502 (2006).
[9] H. Onishi and Y. Iwasawa, Phys. Rev. Lett. **76**, 791 (1996).
[10] R. A. Bennett, P. Stone, N. J. Price, and M. Bowker, Phys. Rev. Lett. **82**, 3831 (1999).
[11] H. Hermann Pieper, K. Venkataramani, S. Torbrügge, S. Bahr, J. V. Lauritsen, F. Besenbacher, A. Kühnle, and M. Reichling, Phys. Chem. Chem. Phys. **12**, 12436 (2010).
[12] M. Li, W. Hebenstreit, and U. Diebold, Phys. Rev. B **61**, 4926 (2000).
[13] M. Blanco-Rey, J. Abad, C. Rogero, J. Méndez, M. López, E. Román, J. Martín-Gago, and P. de Andrés, Phys. Rev. B **75**, 081402 (2007).
[14] N. Shibata, A. Goto, S.-Y. Choi, T. Mizoguchi, S. D. Findlay, T. Yamamoto, and Y. Ikuhara, Science **322**, 570 (2008).
[15] A. R. Oganov and C. W. Glass, J. Chem. Phys. **124**, 244704 (2006).
[16] A. R. Oganov, A. O. Lyakhov, and M. Valle, Acc. Chem. Res. **44**, 227 (2011).
[17] A. O. Lyakhov, A. R. Oganov, H. T. Stokes, and Q. Zhu, Comput. Phys. Commun. **184**, 1172 (2013).
[18] Q. Zhu, L. Li, A. R. Oganov, and P. B. Allen, Phys. Rev. B **87**, 195317 (2013).
[19] V. Sharma *et al.*, Nat. Commun. **5**, 4845 (2014).
[20] See Supplemental Material at http://link.aps.org/supplemental/10.1103/PhysRevLett.113.266101 for the views of metastable reconstructions appear in phase diagram, a more thorough phase diagram, and atomic fractional coordinates of selected reconstructions.
[21] G. Kresse and J. Furthmuller, Phys. Rev. B **54**, 11169 (1996).
[22] G. Kresse and J. Hafner, Phys. Rev. B **48**, 13115 (1993).
[23] C. Di Valentin, G. Pacchioni, and A. Selloni, Phys. Rev. Lett. **97**, 166803 (2006).
[24] J. P. Perdew, K. Burke, and M. Ernzerhof, Phys. Rev. Lett. **77**, 3865 (1996).
[25] P. E. Blochl, Phys. Rev. B **50**, 17953 (1994).
[26] J. Neugebauer and M. Scheffler, Phys. Rev. B **46**, 16067 (1992).
[27] G. Makov and M. C. Payne, Phys. Rev. B **51**, 4014 (1995).
[28] J. Rogal and K. Reuter, Report No. RTO-EN-AVT-142, 2006.
[29] Q.-G. Wang and J.-X. Shang, J. Phys. Condens. Matter **24**, 225005 (2012).
[30] NIST Webbook, http://webbook.nist.gov/.
[31] R. Lindsay, A. Wander, A. Ernst, B. Montanari, G. Thornton, and N. Harrison, Phys. Rev. Lett. **94**, 246102 (2005).
[32] W. Busayaporn *et al.*, Phys. Rev. B **81**, 153404 (2010).
[33] T. Kubo, H. Orita, and H. Nozoye, J. Am. Chem. Soc. **129**, 10474 (2007).
[34] M. Lazzeri and A. Selloni, Phys. Rev. Lett. **87**, 266105 (2001).
[35] C. Pang, S. Haycock, H. Raza, P. Murray, G. Thornton, O. Gülseren, R. James, and D. Bullett, Phys. Rev. B **58**, 1586 (1998).
[36] U. Diebold, J. F. Anderson, K. O. Ng, and D. Vanderbilt, Phys. Rev. Lett. **77**, 1322 (1996).
[37] R. E. Tanner, M. R. Castell, and G. A. D. Briggs, Surf. Sci. **412–413**, 672 (1998).
[38] X. Torrelles, G. Cabailh, R. Lindsay, O. Bikondoa, J. Roy, J. Zegenhagen, G. Teobaldi, W. Hofer, and G. Thornton, Phys. Rev. Lett. **101**, 185501 (2008).
[39] O. Warschkow, Y. Wang, A. Subramanian, M. Asta, and L. D. Marks, Phys. Rev. Lett. **100**, 086102 (2008).
[40] U. Diebold, Surf. Sci. Rep. **48**, 53 (2003).